



UvA-DARE (Digital Academic Repository)

Murchison Widefield Array Limits on Radio Emission from ANTARES Neutrino Events

Croft, S.; Kaplan, D. L.; Tingay, S. J.; Murphy, T.; Bell, M. E.; Rowlinson, A.; MWA Collaboration, [Unknown]; Adrián-Martínez, S.; Ageron, M.; Albert, A.; André, M.; Anton, G.; Ardid, M.; Aubert, J.-J.; Avgitas, T.; Baret, B.; Barrios-Martí, J.; Basa, S.; Bertin, V.; Biagi, S.; Bormuth, R.; Bouwhuis, M.C.; Bruijn, R.; Brunner, J.; Busto, J.; Capone, A.; Caramete, L.; Carr, J.; Chiarusi, T.; Circella, M.; Coleiro, A.; Coniglione, R.; Costantini, H.; Coyle, P.; Creusot, A.; Dekeyser, I.; Deschamps, A.; De Bonis, G.; Distefano, C.; Donzaud, C.; Dornic, D.; Drouhin, D.; Eberl, T.; El Bojaddaini, I.; Elsässer, D.; Enzenhöfer, A.; Fehn, K.; Felis, I.; Fermani, P.; Fusco, L. A.; Galatà, S.; Gay, P.; Geißelsöder, S.; Geyer, K.; Giordano, V.; Gleixner, A.; Glotin, H.; Gracia-Ruiz, R.; Graf, K.; Hallmann, S.; van Haren, H.; Heijboer, A.J.; Hello, Y.; Hernández-Rey, J. J.; Hößl, J.; Hofestädt, J.; Hugon, C.; James, C. W.; de Jong, M.; Kadler, M.; Kalekin, O.; Katz, U.; Kießling, D.; Kooijman, P.; Kouchner, A.; Kreter, M.; Kreykenbohm, I.; Kulikovskiy, V.; Lachaud, C.; Lahmann, R.; Lefèvre, D.; Leonora, E.; Loucatos, S.; Marcelin, M.; Margiotta, A.; Marinelli, A.; Martínez-Mora, J. A.; Mathieu, A.; Michael, T.; Migliozi, P.; Moussa, A.; Mueller, C.; Nezri, E.; Pāvālaš, G. E.; Pellegrino, C.; Perrina, C.; Piattelli, P.; Popa, V.; Pradier, T.; Racca, C.; Riccobene, G.; Roensch, K.; Saldaña, M.; Samtleben, D.F.E.; Sánchez-Losa, A.; Sanguineti, M.; Sapienza, P.; Schmid, J.; Schnabel, J.; Schüssler, F.; Seitz, T.; Sieger, C.; Spurio, M.; Steijger, J.J.M.; Stolarczyk, T.; Taiuti, M.; Tamburini, C.; Trovato, A.; Tselengidou, M.; Turpin, D.; Tönnis, C.; Vallage, B.; Vallée, C.; Van Elewyck, V.; Visser, E.; Vivolo, D.; Wagner, S.; Wilms, J.; Zornoza, J. D.; Zúñiga, J.; ANTARES Collaboration; Klotz, A.; Boer, M.; Le Van Suu, A.; TAROT Collaboration; Akerlof, C.; Zheng, W.; ROTSE Collaboration

DOI

[10.3847/2041-8205/820/2/L24](https://doi.org/10.3847/2041-8205/820/2/L24)

Publication date

2016

Document Version

Final published version

Published in

Astrophysical Journal Letters

[Link to publication](#)



MURCHISON WIDEFIELD ARRAY LIMITS ON RADIO EMISSION FROM ANTARES NEUTRINO EVENTS

S. CROFT^{1,2}, D. L. KAPLAN³, S. J. TINGAY^{4,5}, T. MURPHY^{5,6}, M. E. BELL⁷, A. ROWLINSON^{5,8,9}

(FOR THE MWA COLLABORATION),

S. ADRIÁN-MARTÍNEZ¹⁰, M. AGERON¹¹, A. ALBERT¹², M. ANDRÉ¹³, G. ANTON¹⁴, M. ARDID¹⁰, J.-J. AUBERT¹¹, T. AVGITAS¹⁵,
 B. BARET¹⁵, J. BARRIOS-MARTÍ¹⁶, S. BASA¹⁷, V. BERTIN¹¹, S. BIAGI¹⁸, R. BORMUTH^{19,20}, M. C. BOUWHUIS¹⁹, R. BRUIJN^{19,21},
 J. BRUNNER¹¹, J. BUSTO¹¹, A. CAPONE^{22,23}, L. CARAMETE²⁴, J. CARR¹¹, T. CHIARUSI²⁵, M. CIRCELLA²⁶, A. COLEIRO¹⁵,
 R. CONIGLIONE¹⁸, H. COSTANTINI¹¹, P. COYLE¹¹, A. CREUSOT¹⁵, I. DEKEYSER^{27,28}, A. DESCHAMPS²⁹, G. DE BONIS^{22,23},
 C. DISTEFANO¹⁸, C. DONZAUD^{15,30}, D. DORNIC¹¹, D. DROUHIN¹², T. EBERL¹⁴, I. EL BOJADDAINI³¹, D. ELSÄSSER³²,
 A. ENZENTHÖFER¹⁴, K. FEHN¹⁴, I. FELIS¹⁰, P. FERMANI^{22,23}, L. A. FUSCO^{25,33}, S. GALATÀ¹⁵, P. GAY^{15,34}, S. GEIBELSÖDER¹⁴,
 K. GEYER¹⁴, V. GIORDANO³⁵, A. GLEIXNER¹⁴, H. GLOTIN^{36,37}, R. GRACIA-RUIZ¹⁵, K. GRAF¹⁴, S. HALLMANN¹⁴, H. VAN HAREN³⁸,
 A. J. HELBOER¹⁹, Y. HELLO²⁹, J. J. HERNÁNDEZ-REY¹⁶, J. HÖBL¹⁴, J. HOFESTÄDT¹⁴, C. HUGON^{39,40}, C. W. JAMES¹⁴,
 M. DE JONG^{19,20}, M. KADLER³², O. KALEKIN¹⁴, U. KATZ¹⁴, D. KIEßLING¹⁴, P. KOUIJMAN^{19,21,41}, A. KOUCHNER¹⁵, M. KRETER³²,
 I. KREYKENBOHM⁴², V. KULIKOVSKIY^{18,43}, C. LACHAUD¹⁵, R. LAHMANN¹⁴, D. LEFÈVRE²⁸, E. LEONORA^{35,44}, S. LOUCATOS^{15,45},
 M. MARCELIN¹⁷, A. MARGIOTTA^{25,33}, A. MARINELLI^{46,47}, J. A. MARTÍNEZ-MORA¹⁰, A. MATHIEU¹¹, T. MICHAEL¹⁹, P. MIGLIOZZI⁴⁸,
 A. MOUSSA³¹, C. MUELLER³², E. NEZRI¹⁷, G. E. PÁVÁLAŞ²⁴, C. PELLEGRINO^{25,33}, C. PERRINA^{22,23}, P. PIATTELLI¹⁸, V. POPA²⁴,
 T. PRADIER⁴⁹, C. RACCA¹², G. RICCOBENE¹⁸, K. ROENSCH¹⁴, M. SALDAÑA¹⁰, D. F. E. SAMTLEBEN^{19,20}, A. SÁNCHEZ-LOSA¹⁶,
 M. SANGUINETI^{39,40}, P. SAPIENZA¹⁸, J. SCHMID¹⁴, J. SCHNABEL¹⁴, F. SCHÜSSLER⁴⁵, T. SEITZ¹⁴, C. SIEGER¹⁴, M. SPURIO^{25,33},
 J. J. M. STEIJGER¹⁹, T. STOLARCZYK⁴⁵, M. TAIUTI^{39,40}, C. TAMBURINI²⁸, A. TROVATO¹⁸, M. TSELENGIDOU¹⁴, D. TURPIN¹¹,
 C. TÖNNIS¹⁶, B. VALLAGE^{15,45}, C. VALLÉE¹¹, V. VAN ELEWYCK¹⁵, E. VISSER¹⁹, D. VIVOLO^{48,50}, S. WAGNER¹⁴, J. WILMS⁴²,
 J. D. ZORNOZA¹⁶, J. ZÚÑIGA¹⁶

(FOR THE ANTARES COLLABORATION),

A. KLOTZ^{51,52}, M. BOER⁵³, A. LE VAN SUU⁵⁴

(FOR THE TAROT COLLABORATION),

AND

C. AKERLOF⁵⁵, AND W. ZHENG¹

(FOR THE ROTSE COLLABORATION)

¹ University of California, Berkeley, Astronomy Department, 501 Campbell Hall #3411, Berkeley, CA 94720, USA² Eureka Scientific, Inc., 2452 Delmer Street Suite 100, Oakland, CA 94602, USA³ Department of Physics, University of Wisconsin-Milwaukee, 1900 East Kenwood Boulevard, Milwaukee, WI 53211, USA⁴ International Centre for Radio Astronomy Research, Curtin University, Bentley, WA 6102, Australia⁵ ARC Centre of Excellence for All-sky Astrophysics (CAASTRO), Australia⁶ Sydney Institute for Astronomy, School of Physics, The University of Sydney, NSW 2006, Australia⁷ CSIRO Australia Telescope National Facility, P.O. Box 76, Epping, NSW 1710, Australia⁸ Anton Pannekoek Institute for Astronomy, University of Amsterdam, Science Park 904, 1098 XH Amsterdam, The Netherlands⁹ ASTRON, The Netherlands Institute for Radio Astronomy, Postbus 2, 7990 AA, Dwingeloo, The Netherlands¹⁰ Institut d'Investigació per a la Gestió Integrada de les Zones Costaneres (IGIC)—Universitat Politècnica de València, C/ Paranimf 1, E-46730 Gandia, Spain¹¹ Aix Marseille Université, CNRS/IN2P3, CPPM UMR 7346, F-13288, Marseille, France¹² GRPHE—Université de Haute Alsace—Institut universitaire de technologie de Colmar, 34 rue du Grillenbreit BP 50568-68008 Colmar, France¹³ Technical University of Catalonia, Laboratory of Applied Bioacoustics, Rambla Exposició, E-08800 Vilanova i la Geltrú, Barcelona, Spain¹⁴ Friedrich-Alexander-Universität Erlangen-Nürnberg, Erlangen Centre for Astroparticle Physics, Erwin-Rommel-Str. 1, D-91058 Erlangen, Germany¹⁵ APC, Université Paris Diderot, CNRS/IN2P3, CEA/IRFU, Observatoire de Paris, Sorbonne Paris Cité, F-75205 Paris, France¹⁶ IFIC—Instituto de Física Corpuscular c/ Catedrático José Beltrán, 2 E-46980 Paterna, Valencia, Spain¹⁷ LAM—Laboratoire d'Astrophysique de Marseille, Pôle de l'Étoile Site de Château-Gombert, rue Frédéric Joliot-Curie 38, F-13388 Marseille Cedex 13, France¹⁸ INFN—Laboratori Nazionali del Sud (LNS), Via S. Sofia 62, I-95123 Catania, Italy¹⁹ Nikhef, Science Park, Amsterdam, The Netherlands²⁰ Huygens-Kamerlingh Onnes Laboratorium, Universiteit Leiden, The Netherlands²¹ Universiteit van Amsterdam, Instituut voor Hoge-Energie Fysica, Science Park 105, 1098 XG Amsterdam, The Netherlands²² INFN-Sezione di Roma, P.le Aldo Moro 2, I-00185 Roma, Italy²³ Dipartimento di Fisica e Astronomia dell'Università La Sapienza, P.le Aldo Moro 2, I-00185 Roma, Italy²⁴ Institute for Space Science, RO-077125 Bucharest, Măgurele, Romania²⁵ INFN—Sezione di Bologna, Viale Bertini-Pichat 6/2, I-40127 Bologna, Italy²⁶ INFN—Sezione di Bari, Via E. Orabona 4, I-70126 Bari, Italy²⁷ Mediterranean Institute of Oceanography (MIO), Aix-Marseille University, 13288, Marseille, Cedex 9, France²⁸ Université du Sud Toulon-Var, 83957, La Garde Cedex, CNRS-INSU/IRD UMR 110, France²⁹ Géoazur, Université Nice Sophia-Antipolis, CNRS, IRD, Observatoire de la Côte d'Azur, Sophia Antipolis, France³⁰ Univ. Paris-Sud , F-91405 Orsay Cedex, France³¹ University Mohammed I, Laboratory of Physics of Matter and Radiations, B.P.717, Oujda 6000, Morocco³² Institut für Theoretische Physik und Astrophysik, Universität Würzburg, Emil-Fischer Str. 31, D-97074 Würzburg, Germany³³ Dipartimento di Fisica e Astronomia dell'Università, Viale Bertini Pichat 6/2, I-40127 Bologna, Italy³⁴ Laboratoire de Physique Corpusculaire, Clermont Université, Université Blaise Pascal, CNRS/IN2P3, BP 10448, F-63000 Clermont-Ferrand, France³⁵ INFN—Sezione di Catania, Via S. Sofia, 64, I-95123 Catania, Italy³⁶ LSIS, Aix Marseille Université CNRS ENSAM LSIS UMR 7296, F-13397 Marseille, France³⁷ Université de Toulon CNRS LSIS UMR 7296 83957 La Garde, France; Institut universitaire de France, F-75005 Paris, France³⁸ Royal Netherlands Institute for Sea Research (NIOZ), Landsdiep 4, 1797 SZ't Horntje (Texel), The Netherlands

- ³⁹ INFN—Sezione di Genova, Via Dodecaneso 33, I-16146 Genova, Italy
⁴⁰ Dipartimento di Fisica dell’Università, Via Dodecaneso 33, I-16146 Genova, Italy
⁴¹ Universiteit Utrecht, Faculteit Betawetenschappen, Princetonplein 5, 3584 CC Utrecht, The Netherlands
⁴² Dr. Remeis-Sternwarte and ECAP, Universität Erlangen-Nürnberg, Sternwartstr. 7, D-96049 Bamberg, Germany
⁴³ Moscow State University, Skobeltsyn Institute of Nuclear Physics, Leninskie gory, 119991 Moscow, Russia
⁴⁴ Dipartimento di Fisica ed Astronomia dell’Università, Viale Andrea Doria 6, I-95125 Catania, Italy
⁴⁵ Direction des Sciences de la Matière—Institut de recherche sur les lois fondamentales de l’Univers—Service de Physique des Particules, CEA Saclay, F-91191 Gif-sur-Yvette Cedex, France
⁴⁶ INFN—Sezione di Pisa, Largo B. Pontecorvo 3, I-56127 Pisa, Italy
⁴⁷ Dipartimento di Fisica dell’Università, Largo B. Pontecorvo 3, I-56127 Pisa, Italy
⁴⁸ INFN—Sezione di Napoli, Via Cintia, I-80126 Napoli, Italy
⁴⁹ Université de Strasbourg, IPHC, 23 rue du Loess 67037 Strasbourg, France—CNRS, UMR7178, F-67037 Strasbourg, France
⁵⁰ Dipartimento di Fisica dell’Università Federico II di Napoli, Via Cintia, I-80126 Napoli, Italy
⁵¹ Université de Toulouse; UPS-OMP; IRAP; Toulouse, France
⁵² CNRS; IRAP; 14, avenue Edouard-Belin, F-31400 Toulouse, France
⁵³ ARTEMIS, UMR 7250 (CNRS/OCA/UNS), boulevard de l’Observatoire, BP 4229, F-06304 Nice Cedex, France
⁵⁴ Observatoire de Haute-Provence, F-04870 Saint-Michel l’Observatoire, France
⁵⁵ University of Michigan, 500 East University, Ann Arbor, MI 48109-1120, USA
Received 2016 January 12; accepted 2016 March 6; published 2016 March 22

ABSTRACT

We present a search, using the Murchison Widefield Array (MWA), for electromagnetic (EM) counterparts to two candidate high-energy neutrino events detected by the ANTARES neutrino telescope in 2013 November and 2014 March. These events were selected by ANTARES because they are consistent, within 0.4° , with the locations of galaxies within 20 Mpc of Earth. Using MWA archival data at frequencies between 118 and 182 MHz, taken ~ 20 days prior to, at the same time as, and up to a year after the neutrino triggers, we look for transient or strongly variable radio sources that are consistent with the neutrino positions. No such counterparts are detected, and we set a 5σ upper limit for low-frequency radio emission of $\sim 10^{37}$ erg s $^{-1}$ for progenitors at 20 Mpc. If the neutrino sources are instead not in nearby galaxies, but originate in binary neutron star coalescences, our limits place the progenitors at $z \gtrsim 0.2$. While it is possible, due to the high background from atmospheric neutrinos, that neither event is astrophysical, the MWA observations are nevertheless among the first to follow up neutrino candidates in the radio, and illustrate the promise of wide-field instruments like MWA for detecting EM counterparts to such events.

Key words: neutrinos – radio continuum: general

1. INTRODUCTION

Neutrinos are believed to be emitted by a range of astrophysical sources (Anchordoqui & Montaruli 2010; Chiarusi & Spurio 2010), including transient sources such as gamma-ray bursts (GRBs), core-collapse supernovae (CCSNe), active galactic nuclei (AGNs), and microquasars. Neutrinos provide a powerful probe of high-energy astrophysical environments, because they are unaffected by magnetic fields, and are extremely unlikely to be absorbed by material between the source and the observer. These same properties make them very challenging to detect, even with the largest of the current generation of neutrino observatories, and contaminating background signals are high. However, if their directions can be localized, they have the potential to point directly back to the astrophysical accelerators in which they are created.

Even so, typical positional uncertainties from neutrino telescopes are large enough to encompass many potential EM counterparts. One way to dramatically decrease association ambiguity is to search for transient EM emission that is spatially and temporally consistent with neutrino events. However, aside from neutrinos from the Sun, so far the only astronomical source that has been associated with a neutrino detection (in the tens of MeV energy range) is SN 1987A (Bionta et al. 1987; Hirata et al. 1987; Alexeyev et al. 1988; Pagliaroli et al. 2009). However, Kadler et al. (2016) recently reported a blazar outburst that was coincident with a PeV-energy neutrino event. Timely multi-wavelength follow-up of neutrino candidates is key in order to attempt to identify the progenitors of astrophysical neutrinos.

The two most sensitive neutrino telescopes currently operating are ANTARES (Ageron et al. 2011) and IceCube (Achterberg et al. 2006). Both search for Cherenkov radiation from secondary particles produced from cosmic neutrinos with energies > 100 GeV. For IceCube (IceCube Collaboration 2013), located at the South Pole, neutrinos from the southern sky are observed as downward-going. Below a PeV, these neutrinos are selected with a vetoing technique that favors the detection of showering events, for which the detector has an angular resolution of only 10° – 15° .

ANTARES, located 40 km off the southern coast of France in the Mediterranean Sea, views the southern sky via upward-going neutrino-induced muon tracks, with a characteristic resolution (50% error circle) of 0.4° (Adrián-Martínez et al. 2014). The detector produces the best limits on neutrino emissions for point-like objects in most of this southern sky region, and hence EM follow-up efforts are concentrated there. A dedicated alert system, TAToO (Ageron et al. 2012), is triggered when a candidate special neutrino event is detected: a single high-energy neutrino; a neutrino in the direction of a local galaxy; or at least two neutrinos that are coincident in space and time (Adrián-Martínez et al. 2016).

In this analysis, we searched the MWA archives for observations that were coincident in time and position with neutrino triggers from ANTARES from mid 2013 to mid 2015. Two events, ANT 131121A and ANT 140323A, were found to occur within the MWA field of view (Table 1), when the MWA happened to be observing the trigger position just prior to, during, and immediately after the trigger time.

Table 1

Details of the Two ANTARES Events with Simultaneous MWA Observations

Trigger ID	UT Date	UT Time	R.A. (deg)	Decl. (deg)	Energy (TeV)
ANT 131121A	2013 Nov 21	14:58:28	53.5	-35.1	~1
ANT 140323A	2014 Mar 23	15:31:01	150.9	-27.4	~4

Brief descriptions of the two events and optical follow-up are given in Section 2. The MWA follow-up is presented in Section 3. Limits on progenitors, as well as prospects for future work, are presented in Sections 4 and 5, respectively.

2. ANTARES NEUTRINO EVENTS AND OPTICAL FOLLOW-UP

ANTARES detects 2–3 neutrino candidates per day, on average. From mid 2013 to mid 2015, more than 60 ANTARES events satisfied one of the three special triggers discussed above, and a TAToO alert was issued. For many of these alerts, a network of robotic optical telescopes started observations as soon as possible (prompt strategy) and continued for up to two months (long-term strategy) after the neutrino detection. These strategies are well-suited to the search for rapidly varying transient sources, such as GRB afterglows, and slowly varying sources, such as CCSNe.

Both triggers with simultaneous MWA observations were among the ~30 selected with the ANTARES directional trigger between mid 2013 and mid 2015. Such triggers have directions consistent ($<0.4^\circ$) with the positions (White et al. 2011) of galaxies within 20 Mpc of Earth. Two galaxies match in each case: NGC 1374 and ESO 358-015 match ANT 131121A, and ESO 499-037 and PGC 29194 match ANT 140323A. PGC 29194 (the Antlia Dwarf Galaxy), at a distance of 1.3 Mpc, is located just $6'$ from the neutrino position.

Both neutrino events also had optical follow-up. For ANT 131121A, 12 observations of 6 images were performed with the 0.25 m TAROT telescope in Chile from 2 to 61 days after the trigger. Optical images were analyzed with an image-subtraction pipeline (Adrián-Martínez et al. 2016). No transient was identified, to a limiting magnitude of ~ 19 (S. Adrián-Martínez et al. 2016, in preparation). For ANT 140323A, a total of 8 images were taken with ROTSE 3b in Texas (starting ~ 15 hr after the trigger) according to the prompt strategy, and 10 images were taken with TAROT Chile up to 45 days after the trigger according to the long-term strategy. No transient counterpart was found (S. Adrián-Martínez et al. 2016, in preparation; Adrián-Martínez et al. 2016), to limiting magnitudes of 16.4 (prompt) and 18.7 (long-term).

3. MWA FOLLOW-UP OF ANTARES EVENTS

The Murchison Widefield Array (MWA), situated in Western Australia, is the Square Kilometre Array precursor at low (80–300 MHz) radio frequencies (Lonsdale et al. 2009; Tingay et al. 2013). The MWA is often used to undertake surveys, for a range of science goals including dedicated (e.g., Bell et al. 2014; Murphy et al. 2015) and commensal (e.g., Rowlinson et al. 2016; Tingay et al. 2015) transient searches, but it has also been used for triggered follow-up of transients at other wavelengths (e.g., Kaplan et al. 2015). Its huge field of view (700 square degrees at 150 MHz) also means that archival observations have a much larger chance, compared to most

other radio telescopes, of serendipitously covering an event of interest. This capability is particularly valuable for follow-up of neutrino or gravitational wave (Singer et al. 2015) candidates, which have rather large position uncertainties.

We obtained MWA archival data for both ANTARES triggers, from periods before (Section 3.2) and at the time of (Section 3.1) the trigger, in a search for prompt emission. We also searched for data over a longer range of time to look for late-time emission (Section 3.3).

Flagged CASA (McMullin et al. 2007) measurement sets were produced using the MWA preprocessing pipeline COTTER (Offringa et al. 2015). These were then processed by our custom imaging pipeline, which used WSCLEAN (Offringa et al. 2014) with 40,000 CLEAN iterations to produce XX and YY polarization images with 3072×3072 0.9 pixels. The images were amplitude and phase self-calibrated, and primary beam-corrected to produce Stokes I images, which formed the basis for our analysis. Catalogs were generated using Aegean (Hancock et al. 2012) and cross-matched across snapshots.

3.1. Search for Prompt Emission

For each of the two triggers, we retrieved 34 MWA data sets, in addition to observations of nearby bright radio calibrators (Pic A for ANT 131121A and Hyd A for ANT 140323A). Exposure times were 112 s, and snapshots were taken approximately every 2 minutes, from ~ 10 minutes before the neutrino trigger to 1 hr after (sufficiently long to probe dispersion measures $> 10^4$ pc cm $^{-3}$). For ANT 131121A, the central frequency for each observation was 154.255 MHz, and the bandwidth was 30.72 MHz, divided into 768 channels of 40 kHz. ANT 140323A had the same bandwidth and channels, but the central frequency was 182.415 MHz. The MWA synthesized beam is $\sim 2' \times 2'$ at 154 MHz.

Of the 34 snapshots for ANT 131121A, 1 failed to image adequately and was discarded. Comparison by eye of the remaining snapshot images for each trigger showed no obvious transients to be present in or near the ANTARES 90% error circles, which are 1° in radius (Adrián-Martínez et al. 2014). Additionally, no transients (sources ≥ 5 times brighter than the background fluctuations) were present in catalogs corresponding to a single snapshot within the ANTARES error circles.

We extracted square image cutouts 5° on a side centered on the trigger positions, and combined these, taking the median value at each pixel position, to create a deep image for each trigger (center panels of Figure 1). We also measured the rms flux density in the object-subtracted background sky, σ_{sky} (which corresponds to the sensitivity), in the $5^\circ \times 5^\circ$ regions centered on each trigger. The flux density for the faintest detectable source was set at $4\sigma_{\text{sky}}$.

The mean σ_{sky} of the 33 ANT 131121A prompt snapshot images was 48 mJy beam $^{-1}$, and the standard deviation of σ_{sky} for these images was 4 mJy beam $^{-1}$. The 34 ANT 140323A prompt snapshots had $\sigma_{\text{sky}} = 87 \pm 7$ mJy beam $^{-1}$. For ANT 131121A, σ_{sky} for the deep image made from the 33 snapshots should naively correspond to $48/\sqrt{33} = 8$ mJy beam $^{-1}$. After the snapshots have been median-combined (i.e., the median at each pixel is used), however, the measured σ_{sky} is somewhat higher (18 mJy beam $^{-1}$) than the naive expectation, due to the presence of sidelobes and confused sources (Wayth et al. 2015). Similarly, for ANT 140323A we obtained

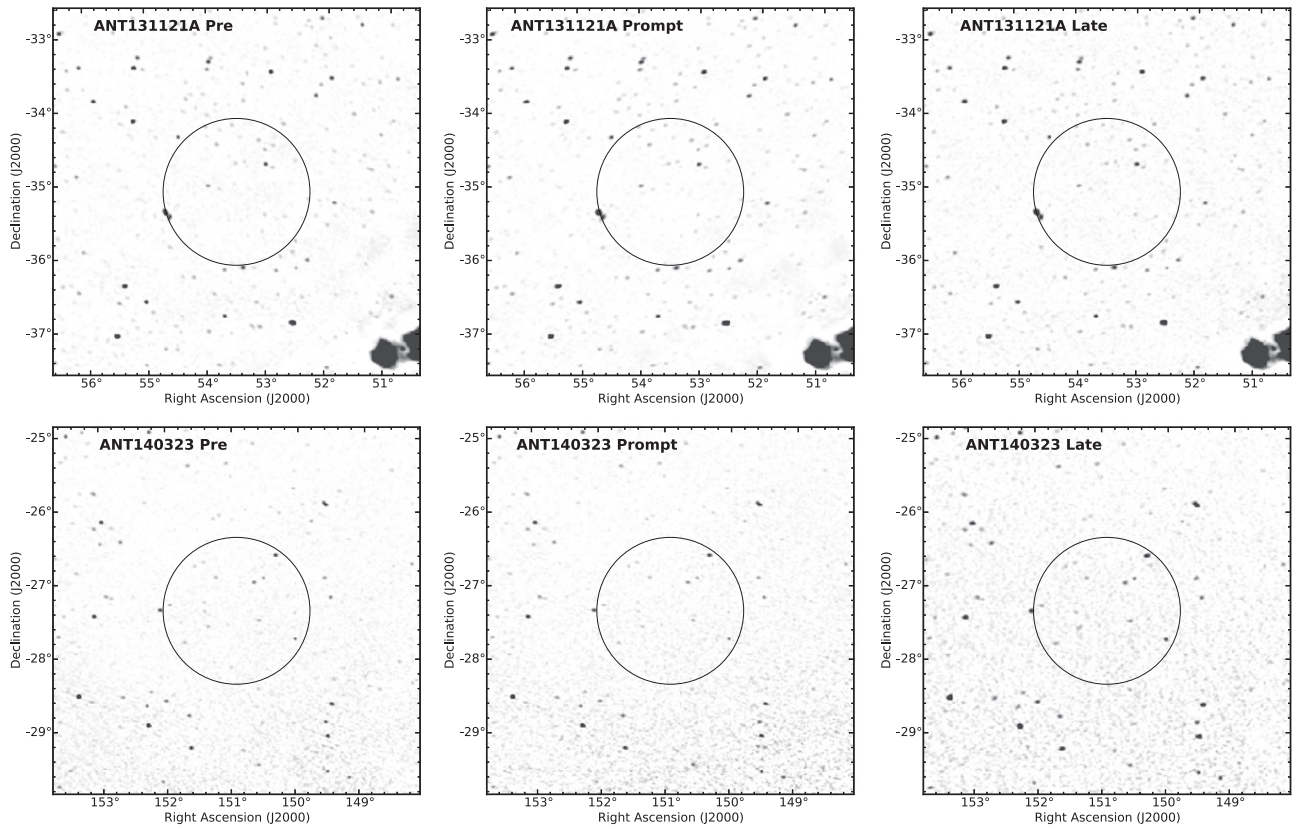


Figure 1. $5^\circ \times 5^\circ$ cutouts from median-combined deep images on each of the two triggers (top: ANT 131121A; bottom: ANT 140323A). From left to right, images were taken ~ 20 days prior to, at the time of, and over the course of ~ 1 year after the trigger time (Table 2). Some faint image artifacts are visible, particularly in the top panels around the bright source Fornax A. In the bottom panels, enhanced noise is visible toward the bottom due to the effects of the fall-off in sensitivity toward the edge of the primary beam. The grayscale runs from 0 to 1 Jy beam $^{-1}$. The 90% ANTARES error circles (radius 1°) are shown.

47 mJy beam $^{-1}$ for the deep median-combined image. The difference in sensitivity between the two fields is partly because of the difference in frequencies, and partly because ANT 140323A is closer to the edge of the MWA primary beam than ANT 131121A, resulting in higher σ_{sky} .

3.2. Pre-trigger Comparison Images

We also retrieved archival MWA data from ~ 20 days prior to each trigger. For ANT 131121A we obtained 30 observations at 154 MHz from UT 2013 November 1. For ANT 140323A we obtained 31 observations at 182 MHz from UT 2014 March 2. These were analyzed in the same manner as described above. Deep images made from combining the ~ 1 hr of observations for each trigger are shown in the left panels of Figure 1. Comparison of the pre-trigger and prompt deep images by eye again showed no obvious transients.

We used the matched snapshot catalogs (independently for the pre-trigger and prompt data sets) to measure the mean (\bar{S}) and standard deviation (σ_S) of the flux densities of radio sources detected in our data. For all sources detected in at least 10 of the ~ 30 snapshots, we computed variability statistics (reduced chi-squared, χ_ν^2 , and fractional modulation, σ_S/\bar{S}). In Figure 2, we plot χ_ν^2 versus σ_S/\bar{S} for these sources. Varying image quality and detection thresholds make the comparison challenging, but if a trigger was associated with strong variability in an existing radio source, we might expect to see an outlier with high χ_ν^2 and fractional modulation in the prompt data set, but not in the corresponding pre-trigger data set.

The majority of the points in our variability plots occupy a contiguous region of parameter space, with brighter sources tending to be detected in more snapshots, and having higher χ_ν^2 , as would be expected given improved signal to noise for these sources. Very few well-detected sources (those seen in ~ 30 snapshots) exhibit $\sigma_S/\bar{S} \gtrsim 50\%$, with the exception of the largest (i.e., brightest) two points in the ANT 131121A prompt plot, which have $\sigma_S/\bar{S} = 0.59$ and 0.55 , respectively. Both have $\chi_\nu^2 \approx 10$, suggesting that they are indeed strongly variable. However, both are coincident with the lobes of Fornax A, and while AGN cores can sometimes vary on short timescales, extended lobes cannot. We therefore conclude that the apparent variability here is caused by the difficulty of fitting point source models to extended emission. Variations in sensitivity and image quality result in different fits at each epoch, which is also why these sources do not appear in the same position in the top left panel of Figure 2. In any case, Fornax A is too far from the trigger position, given the ANTARES positional uncertainties, to be the neutrino source (likelihood of association $\sim 5 \times 10^{-4}$).

The plots for ANT 140323A show fewer sources, due to the poorer sensitivity associated with the location of this candidate toward the edge of the primary beam. Nevertheless, there are no well-detected sources that appear as outliers in the prompt data and not in the pre-trigger data. We conclude, therefore, that our observations did not convincingly detect any strong AGN flares associated with the neutrino triggers.

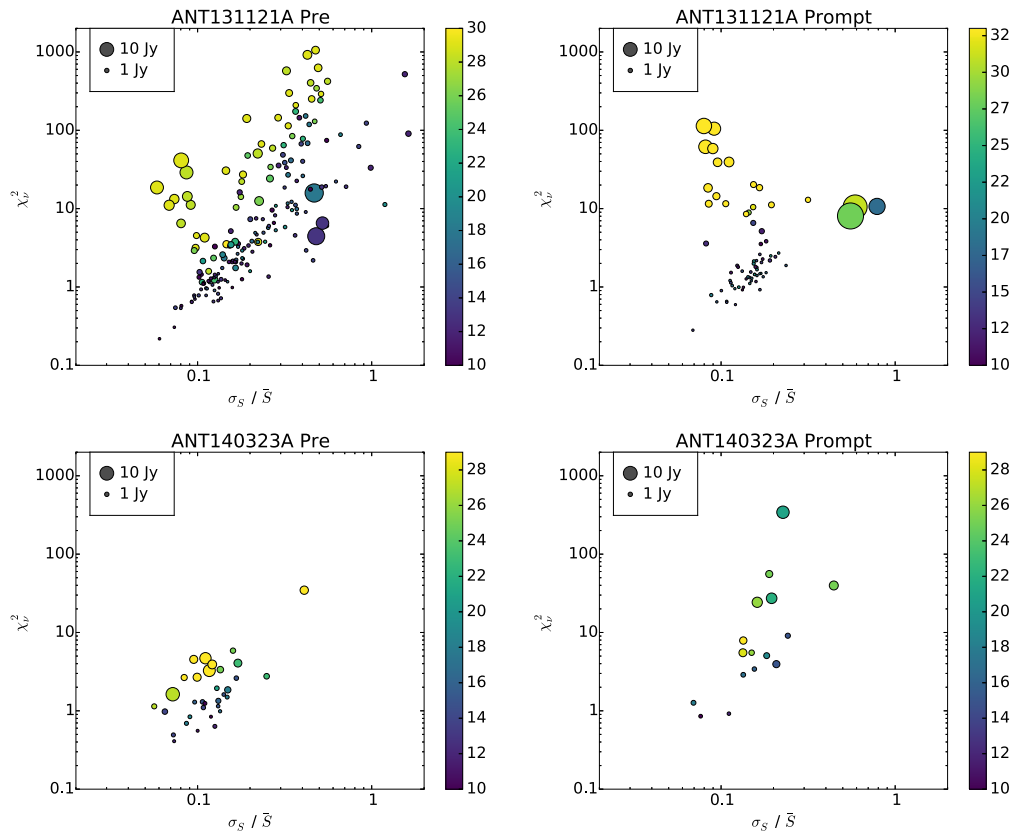


Figure 2. Reduced chi-squared, χ_{ν}^2 , for the hypothesis that sources do not vary over the ~ 30 snapshots, plotted against fractional modulation (standard deviation, σ_S , divided by the mean, \bar{S} , flux density for the same sources). Sources are color-coded according to the number of snapshots in which they were detected. Data are plotted for the pre-trigger (left) and prompt (right) data sets, for ANT 131121A (top) and ANT 140323A (bottom). Only sources detected in ≥ 10 of the snapshot images for each data set are shown. Circle sizes scale with \bar{S} .

3.3. Search for Late-time Emission

The MWA observing strategy, particularly changes in programs from one season to the next, somewhat restricts our ability to obtain a long-timescale follow-up of any given position of interest by simply searching the archive (as opposed to undertaking a dedicated follow-up campaign). Nevertheless, we were able to retrieve observations for both triggers that can be used to constrain late-time emission. We searched the archive for observations evenly distributed in $\log(\text{time})$: 1, 2, 4, ..., 8192 hr after the trigger. In most cases we were able to find data close in time to the desired epoch (Table 2). When no suitable data were present in the archive that were closer in $\log(\text{time})$ to a given epoch than to the previous or next epoch, that epoch was skipped.

Images were produced in the same manner as described above. Snapshot image sensitivity (which can be sensitive to the inclusion of relatively small amounts of poor quality data), σ_{sky} , ranged from 49–373 mJy beam $^{-1}$ (Table 2). Once again, we made deep images (right panels of Figure 1) by median-combining snapshots. Since the snapshots were taken over a wide range in time (see Table 2), the median will de-emphasize sources that vary with a characteristic timescale of $\ll 1$ year. These images nevertheless provide good sensitivity to long-timescale transient or variable sources associated with the neutrino.

Once again, neither trigger had an obvious transient counterpart, either in the snapshots, or in the deep images.

4. LIMITS ON PROGENITORS

ANTARES detects ~ 2 atmospheric neutrinos per day with energies comparable to our two events ($\gtrsim 1$ TeV). However, both candidates were generated by the ANTARES directional trigger (Section 2), having positions coincident with galaxies within 20 Mpc. Such coincidences represent $\sim 2\%$ of the background from atmospheric events (Adrián-Martínez et al. 2016). If we assume that the ANTARES neutrinos are indeed astrophysical, rather than due to terrestrial backgrounds, we can use our data to place some of the first low-frequency radio limits on EM counterparts to neutrino events. If the nearby galaxies are the hosts of the neutrino progenitors, this allows us to place limits on the luminosity of any EM counterpart.

Using 5σ upper limits of 90–340 mJy (based on σ_{sky} for the deep images in Table 2, which ranges from 18 to 68 mJy beam $^{-1}$), we obtain $L_{150 \text{ MHz}} \lesssim 10^{29} \text{ erg s}^{-1} \text{ Hz}^{-1}$ ($\lesssim 10^{37} \text{ erg s}^{-1}$) for progenitors at 20 Mpc. These limits do not strongly constrain late-time emission from even the most luminous radio supernovae or GRBs at these distances; during the first ~ 100 days after the event, radio emission at MWA frequencies would be expected to be $\lesssim 10^{28} \text{ erg s}^{-1} \text{ Hz}^{-1}$ (Soderberg et al. 2010). Our limits are better ($\lesssim 10^{27} \text{ erg s}^{-1} \text{ Hz}^{-1}$) if ANT 140323A is associated with the Antlia Dwarf at 1.3 Mpc, but this still does not provide a strong constraint on progenitors. In fact, due to synchrotron self-absorption at low radio frequencies, late-time emission tends to be faint in general (e.g., Metzger et al. 2015), further

Table 2
Limits on Radio Counterparts

UT Date	UT Time	Time Since Trigger (hr)	Frequency (MHz)	σ_{sky} (mJy beam ⁻¹)
ANT 131121A				
2013 Nov 1 average ^a	18:15:12	-477	154	24
2013 Nov 21 average ^a	14:50:56	0	154	18
2013 Nov 21 ^b	16:59:04	2	154	49
2013 Nov 21 ^b	18:36:40	4	154	93
2013 Nov 22 ^b	14:47:04	24	154	51
2013 Nov 26 ^b	18:16:56	123	154	201
2013 Dec 3 ^b	14:18:56	287	154	50
2013 Dec 6 ^b	15:25:28	360	154	200
2014 Feb 14 ^b	13:00:56	2038	182	337
2014 Jul 20 ^b	22:20:24	5791	182	48
2014 Oct 28 ^b	16:48:24	8185	118	70
Late-time average ^a	...	2-8185	118, 154, 182	34
ANT 140323A				
2014 Mar 2 average ^a	16:20:16	-503	182	36
2014 Mar 23 average ^a	15:21:12	0	182	47
2014 Mar 24 ^b	12:36:40	21	154	133
2014 Mar 24 ^b	16:24:24	24	154	176
2014 Mar 26 ^b	12:28:48	68	154	143
2014 Mar 28 ^b	16:08:40	120	154	196
2014 Apr 3 ^b	11:57:20	260	154	135
2014 Apr 13 ^b	15:05:44	503	154	178
2014 May 5 ^b	10:31:12	1027	154	93
2014 Oct 25 ^b	21:34:00	5190	154	373
2015 Feb 26 ^b	15:41:20	8160	154	68
Late-time average ^a	...	21-8160	154	68

Notes.

^a Deep images made from median-combining snapshot images.

^b Individual late-time snapshot images.

emphasizing the need for rapid response or simultaneous observations to search for brighter prompt radio emission.

For GRBs or CCSNe at distances < 20 Mpc, we consider whether counterparts should have been seen in the optical observations (Section 2). At 20 Mpc, the optical limit of 18.7 mag corresponds to absolute magnitudes brighter than -13 , sensitive enough to detect all but the faintest (e.g., Pastorello et al. 2007) supernovae, although this does not account for dust obscuration in the host galaxy. We also consider a scenario where the nearby galaxies are chance alignments, and the progenitors are in fact at larger distances. Considering the possibility that the neutrinos might be from binary neutron star coalescences such as those modeled by Pshirkov & Postnov (2010), our upper limits for prompt emission, with their Equation (8) and assuming an efficiency scaling exponent $\gamma = 0$, would place such progenitors at distances of $\gtrsim 1$ Gpc ($z \gtrsim 0.2$).

5. OUTLOOK

Although the MWA has excellent capabilities for these kinds of serendipitous searches due to its wide field of view, the use

of archival data has limitations. Neither trigger was optimally placed within the MWA field of view: ANT 131121A was $\sim 8^\circ$ from the pointing center, and ANT 140323A was $\sim 17^\circ$ away. Particularly in the latter case, the fall-off in primary beam response means that noise in the region of the image near the trigger position is higher than is ideal. Going forward, we intend to trigger pointed observations soon after a neutrino detection. The region of sky seen from the MWA is well-matched to where ANTARES has good sensitivity, meaning that around 40% of ANTARES upward-going events are accessible to rapid MWA follow-up. ANTARES can generate triggers in a few seconds, and MWA can point at the trigger position within another 10 s, allowing us to probe dispersion measures as low as 100 pc cm^{-3} (Kaplan et al. 2015), sufficiently fast to detect even minimally dispersed events from the nearest galaxies. The MWA's wide field of view also means that targeted follow-up observations easily probe the entire error circle of ANTARES events with optimal MWA sensitivity.

It is notable that Fornax A, one of the brightest radio sources in the sky (associated with NGC 1316 at a distance of ~ 20 Mpc) is close ($\sim 3^\circ$) to the position of ANT 131121A, although it is strongly ruled out as the progenitor given the positional uncertainties of the ANTARES trigger. However, this region of the sky is densely populated with galaxies (including ~ 10 bright members of the Fornax Cluster within the neutrino error circle), illustrating the importance of EM observations that are coincident in time with neutrino triggers to resolve ambiguity as to the progenitor.

Although we found no strongly varying radio counterpart to the two triggers discussed here, MWA data at the positions of additional ANTARES triggers exist in our archive, albeit they are not simultaneous in time with the triggers. We defer the analysis of late-time and pre-trigger observations of these events to a future paper. Additionally, future rapid follow-up (a capability already demonstrated at MWA), combined with an increase in sensitivity (due to a decrease in the confusion limit from the recently approved MWA expansion), mean that MWA is well positioned to follow up with promising neutrino candidates over the next few years.

This scientific work makes use of the Murchison Radio-astronomy Observatory, operated by CSIRO. We acknowledge the Wajarri Yamatji people as the traditional owners of the Observatory site. Support for the operation of the MWA is provided by the Australian Government Department of Industry and Science and Department of Education (National Collaborative Research Infrastructure Strategy: NCRIS), under a contract with Curtin University, administered by Astronomy Australia Limited. We acknowledge the iVEC Petabyte Data Store and the Initiative in Innovative Computing and the CUDA Center for Excellence sponsored by NVIDIA at Harvard University. D.L.K. and S.D.C. acknowledge support from the US National Science Foundation (grant AST-1412421). We acknowledge the financial support of the funding agencies: Centre National de la Recherche Scientifique (CNRS), Commissariat à l'énergie atomique et aux énergies alternatives (CEA), Commission Européenne (FEDER fund and Marie Curie Program), Région Ile-de-France (DIM-ACAV), Région Alsace (contrat CPER), Région Provence-Alpes-Côte d'Azur, Département du Var and Ville de La Seyne-sur-Mer, France; Bundesministerium für Bildung und

Forschung (BMBF), Germany; Istituto Nazionale di Fisica Nucleare (INFN), Italy; Stichting voor Fundamenteel Onderzoek der Materie (FOM), Nederlandse organisatie voor Wetenschappelijk Onderzoek (NWO), the Netherlands; Council of the President of the Russian Federation for Young Scientists and Leading Scientific Schools Supporting Grants, Russia; National Authority for Scientific Research (ANCS), Romania; Ministerio de Ciencia e Innovación (MICINN), Prometeo of Generalitat Valenciana and MultiDark, Spain; Agence de l'Oriental and CNRST, Morocco. We also acknowledge the technical support of Ifremer, AIM, and Foselev Marine for the sea operation and the CC-IN2P3 for the computing facilities. We gratefully acknowledge financial support from the OCEVU LabEx, France. We thank Nathan Whitehorn and the anonymous referee for helpful comments.

REFERENCES

- Achterberg, A., Ackermann, M., Adams, J., et al. 2006, *APh*, **26**, 155
- Adrián-Martínez, S., Ageron, M., Albert, A., et al. 2016, *JCAP*, **02**, 062
- Adrián-Martínez, S., Albert, A., André, M., et al. 2014, *ApJL*, **786**, L5
- Ageron, M., Aguilar, J., Samarai, I. A., et al. 2011, *NIMPA*, **656**, 11
- Ageron, M., Aguilar, J. A., Al Samarai, I., et al. 2012, *Aph*, **35**, 530
- Alexeyev, E. N., Alexeyeva, L. N., Krivosheina, I. V., & Volchenko, V. I. 1988, *PhLB*, **205**, 209
- Anchordoqui, L. A., & Montaruli, T. 2010, *ARNPS*, **60**, 129
- Bell, M. E., Murphy, T., Kaplan, D. L., et al. 2014, *MNRAS*, **438**, 352
- Bionta, R. M., Blewitt, G., Bratton, C. B., Casper, D., & Ciocio, A. 1987, *PhRvL*, **58**, 1494
- Chiarusi, T., & Spurio, M. 2010, *EPJC*, **65**, 649
- Hancock, P. J., Murphy, T., Gaensler, B. M., Hopkins, A., & Curran, J. R. 2012, *MNRAS*, **422**, 1812
- Hirata, K., Kajita, T., Koshiba, M., Nakahata, M., & Oyama, Y. 1987, *PhRvL*, **58**, 1490
- IceCube Collaboration 2013, *Sci*, **342**, 1242856
- Kadler, M., Krauß, F., Mannheim, K., et al. 2016, *NatPh*, in press (arXiv:1602.02012)
- Kaplan, D. L., Rowlinson, A., Bannister, K. W., et al. 2015, *ApJL*, **814**, L25
- Lonsdale, C. J., Cappallo, R. J., Morales, M. F., et al. 2009, *IEEEP*, **97**, 1497
- McMullin, J. P., Waters, B., Schiebel, D., Young, W., & Golap, K. 2007, in *ASP Conf. Ser. 376, Astronomical Data Analysis Software and Systems XVI*, ed. R. A. Shaw, F. Hill, & D. J. Bell (San Francisco, CA: ASP), 127
- Metzger, B. D., Williams, P. K. G., & Berger, E. 2015, *ApJ*, **806**, 224
- Murphy, T., Bell, M. E., Kaplan, D. L., et al. 2015, *MNRAS*, **446**, 2560
- Offringa, A. R., McKinley, B., Hurley-Walker, N., et al. 2014, *MNRAS*, **444**, 606
- Offringa, A. R., Wayth, R. B., Hurley-Walker, N., et al. 2015, *PASA*, **32**, 8
- Pagliaroli, G., Vissani, F., Costantini, M. L., & Ianni, A. 2009, *Aph*, **31**, 163
- Pastorello, A., Della Valle, M., Smartt, S. J., et al. 2007, *Natur*, **449**, 1
- Pshirkov, M. S., & Postnov, K. A. 2010, *Ap&SS*, **330**, 13
- Rowlinson, A., Bell, M. E., Murphy, T., et al. 2016, *MNRAS*, in press
- Singer, L. P., Kasliwal, M. M., Cenko, S. B., et al. 2015, *ApJ*, **806**, 52
- Soderberg, A. M., Chakraborti, S., Pignata, G., et al. 2010, *Natur*, **463**, 513
- Tingay, S. J., Goeke, R., Bowman, J. D., et al. 2013, *PASA*, **30**, 7
- Tingay, S. J., Trott, C. M., Wayth, R. B., et al. 2015, *AJ*, **150**, 199
- Wayth, R. B., Lenc, E., Bell, M. E., et al. 2015, *PASA*, **32**, 25
- White, D. J., Daw, E. J., & Dhillon, V. S. 2011, *CQGrA*, **28**, 085016